Biochimica et Biophysica Acta 1838 (2014) 3203–3211

Contents lists available at ScienceDirect

Biochimica et Biophysica Acta

journal homepage: www.elsevier.com/locate/bbamem

Functional characterization of the CDF transporter SMc02724 (SmYiiP) in *Sinorhizobium meliloti*: Roles in manganese homeostasis and nodulation

Daniel Raimunda *, Graciela Elso-Berberián

Instituto de Investigación Médica Mercedes y Martín Ferreyra (INIMEC), Consejo Nacional de Investigaciones Científicas y Técnicas (CONICET), Universidad Nacional de Córdoba, Córdoba, Argentina

ARTICLE INFO

Article history:
Received 16 May 2014
Received in revised form 11 September 2014
Accepted 12 September 2014
Available online 19 September 2014

Keywords:
Cation diffusion facilitator
Manganese homeostasis
Manganese efflux
Sinorhizobium meliloti

ABSTRACT

In bacteria, membrane transporters of the cation diffusion facilitator (CDF) family participate in Zn^{2+}, Fe^{2+}, Mn^{2+}, Co^{2+} and Ni^{2+} homeostasis. The functional role during infection processes for several members has been shown to be linked to the specificity of transport. *Sinorhizobium meliloti* has two homologous CDF genes with unknown transport specificity. Here we evaluate the role played by the CDF SMc02724 (SmYiiP). The deletion mutant strain of SmYiiP (Δ*smyiiP*) showed reduced in vitro growth fitness only in the presence of Mn^{2+}. Incubation of Δ*smyiiP* and WT cells with sub-lethal Mn^{2+} concentrations resulted in a 2-fold increase of the metal only in the mutant strain. Normal levels of resistance to Mn^{2+} were attained by complementation with the gene SMc02724 under regulation of its endogenous promoter. In vitro, liposomes with incorporated heterologously expressed pure protein accumulated several transition metals. However, only the transport rate of Mn^{2+} was increased by imposing a transmembrane H^+ gradient. Nodulation assays in alfalfa plants showed that the strain Δ*smyiiP* induced a lower number of nodules than in plants infected with the WT strain. Our results indicate that Mn^{2+} homeostasis in *S. meliloti* is required for full infection capacity, or nodule function, and that the specificity of transport in vivo of SmYiiP is narrowed down to Mn^{2+} by a mechanism involving the proton motive force.

1. Introduction

Transition metals (Cu, Fe, Ni, Co, Mn) are key components of essential metalloproteins in all living organisms. Their ubiquitous requirement mirrors the ability of cells to finely tune and regulate their chemical properties through ligand coordination in catalytic or structural metal binding sites. However, these elements become noxious for particular organisms beyond the upper level limits of the cellular requirement. In some cases, this is due to their ability to generate reactive oxygen species via Fenton-like reactions, compromising cellular structural elements [1], or by inactivating important metabolic enzymes containing [Fe–S] clusters [2,3]. Importantly, the orchestration of transcriptional regulators, transporters and metallochaperones allows fast and efficient influx or efflux, and the compartmentalization of these micronutrients to supply cellular demands.

In bacteria, several families of membrane proteins (importers and exporters) contribute to maintaining adequate quotas of transition metals. This assures metalloprotein synthesis by restraining levels between normal ranges. However, recent findings show that a different type of transporter can contribute to the correct trafficking and delivery of the metal to a specific metal binding site in a partner protein [4,5]. In each case, the potential toxic effects of general protein dysfunction by mismetallation, when a transition metal is abundant, or by the lack of specific metallation, when the cognate metal is scarce, are bypassed. Both of these roles have been shown to be important in infection processes. For example, it was demonstrated that homologous Cu^+-ATPases in *P. aeruginosa*, named CopA1 and CopA2, performed different roles participating in mechanisms that involve metal detoxification (driven by CopA1), or cytochrome c oxidase metallation (driven by CopA2), but their single deletion resulted in a similarly attenuated virulent phenotype [4].

The cation diffusion facilitator (CDF) family transporters are polytopic membrane proteins that are key for bacterial physiology. Members of the family function as exporters of divalent metal cations and their roles in bacteria have mainly been assigned to transition metal detoxification [6,7]. Transport mechanism studies have proposed a counter transport mechanism, driven by K^+/H^+ electrochemical gradients and membrane potential [7–9]. Biochemical and structural works suggest that bacterial CDF transporters become functional when two monomers are linked at the cytoplasmic membrane interface by intermolecular stabilization of charges [10]. Each monomer has 6 transmembrane segments (TM), and both C- and N-terminal domains

Abbreviations: CDF, cation diffusion facilitator; TM, transmembrane; CTD, C-terminal domain; NTD, N-terminal domain; DDM, dodecyl-β-D-maltoside; NMG, N-Methyl-D-glucamine; MES, 2-(N-Morpholino)ethanesulfonic acid; TEV, tobacco etch virus; ICP-MS, inductively coupled plasma mass spectrometry

* Corresponding author at: Instituto de Investigación Médica Mercedes y Martín Ferreyra, Friuli 2434, Córdoba, C.P. 5016, Argentina. Tel.: +54 351 4681465; fax: +54 351 4695163.
E-mail address: draimunda@immf.uncor.edu (D. Raimunda).

http://dx.doi.org/10.1016/j.bbamem.2014.09.005
0005-2736/

(C-NTD) are cytosolic. The αßßαß folding found in CTD resembles that observed in metallochaperones and regulatory domains, suggesting a role in regulation or metal delivery to the transport site [11]. The X-ray crystal structure of the *Escherichia coli* YiiP CDF transporter, in the outward (metal bound) conformation, depicts 3 metal binding sites (A, B and C) [10]. Site A is important for transport and specificity [12]. In YiiP, site A is formed by two Asp in TM2 and a His and Asp in TM5, resulting in tetrahedral coordination of Zn^{2+} [10]. Fe^{2+} has also been proposed as the transport substrate for YiiP [7]. Sites B and C at the CTD would participate in transport or regulation. Pointing to a critical role during infectious processes, a deletion mutant of the only CDF member in *Streptococcus pneumonia*, MntE (Sp1555), led to decreased virulence in a mice infection model. Although a specific mechanism was not proposed, it was postulated that MntE is a Mn^{2+} exporter [13].

Recent phylogenetic analyses based on amino acid sequence alignment have shown that previously characterized members with small variations, if any, in the residues participating in transport site A, result in a wide range of transported substrates. Even members of the same clade seem to transport different metals [14]. Cubillas et al. have proposed that the specificity is achieved not only within the constraints imposed by the amino acid sequence at the transport site, but also in determinants probably found at the secondary sphere of coordination.

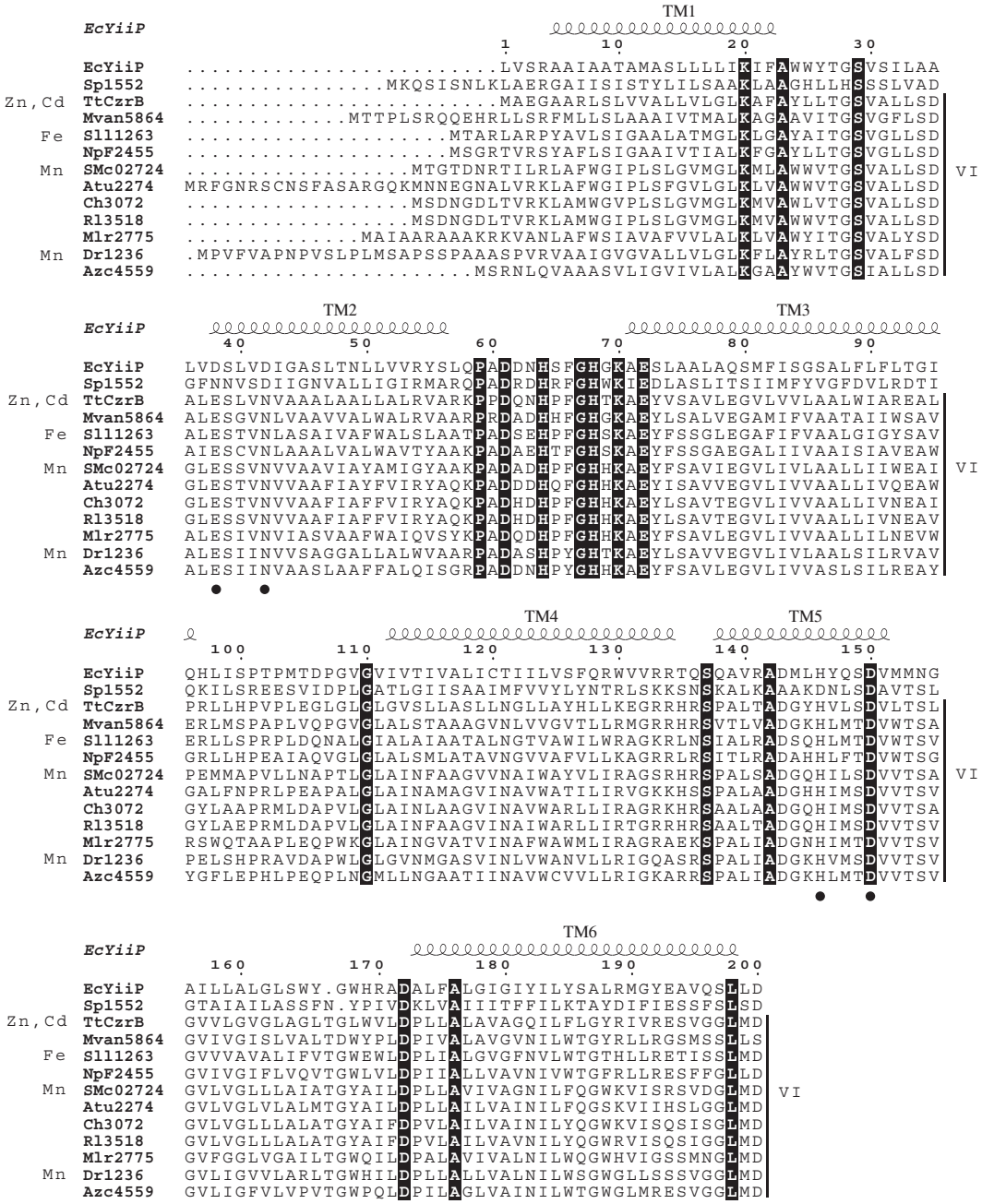

Fig. 1. Protein sequence alignment of CDF members. Organisms and locus names used are: *Thermus thermophilus*, TtCzrB; *Mycobacterium vanbaalenii* PYR-1, Mvan_5864; *Synechocystis sp.* PCC 680, Sll1263; *Nostoc punctiforme* PCC 73102, NpF2455; *Sinorhizobium meliloti*, Rm1021, SMc02724; *Agrobacterium tumefaciens* str. C58, Atu2274; *Rhizobium etli* CFN 42, Ch3072; *Rhizobium leguminosarum* bv. viciae 3841, Rl3518; *Mesorhizobium loti* MAFF303099, Mlr2775; *Deinococcus radiodurans* R1, Dr1236; and *Azorhizobium caulinodans* ORS 571, Azc4559. Only transmembrane segments (TM) are shown for comparison. *E. coli* YiiP/FieF and *S. pneumonia* Sp1552 are included and members of the clade VI [14] are denoted with a black bar on the right. Metal transport specificity for each sub-group is indicated on the right (Zn, Fe, Cd, Mn). Black dots (●) on TM2 and TM5 indicate the transport binding site amino acids characterized previously in EcYiiP. Conserved residues are shown in black boxes.

Table 1
List of strains and plasmids used in this work.

Strains	Relevant characteristics	Reference
Sinorhizobium meliloti		
Rm1021	Wild-type (Str^R)	Luo et al. [22]
Δ*smyiiP*	SMc02724::pK19mob2ΩHMB-G1PELR22D11 (Str^R) (Kan^R)	This work
Δ*smyiiP-rhaS*::P-SmYiiP	SMc02724::pK19mob2ΩHMB-G1PELR22D11, *rhaS*::pCAP77-P-SMc02724 (Str^R) (Kan^R) (Rha-)	This work
Escherichia coli		
S17-1	*E. coli 294, thi RP4-2-Tc::Mu-Km::Tn7* chromosomally integrated	Simon et al. [21]
DH5α	F-*Φ80lacZΔM15 Δ(lacZYA-argF) U169 recA1 endA1 hsdR17 (rK–, mK +) phoA supE44 λ–thi-1 gyrA96 relA1*	Invitrogen, Carlsbad, CA, USA
BL21(DE3)pLysS	F-*ompT hsdS*B (rB−mB−) *gal dcm* (DE3) *pLysS* (Cam^R)	Invitrogen, Carlsbad, CA, USA
Plasmids		
pK19mob2ΩHMB	RP4 mobilizable plasmid, Kan	Luo et al. [22]
pCAP77	*rha* insertion plasmid, pMB438, *trp* terminator, Nm	Arango-Pinedo et al. [23]
pK19mob2ΩHMB-G1PELR22D11	SMc02724 insertion plasmid	www.rhizogate.de
pCAP77-P-SMc02724	*rha* insertion plasmid containing gene locus SMc02724 plus 500 bp upstream (P, promoter)	This work

The *Sinorhizobium meliloti* genome has two homologous CDF genes, SMc02724 and SMc04167, of unknown transport specificity and biological roles. In order to predict the substrate specificity of SMc02724, we analyzed the protein sequence alignment, including previously characterized orthologs from available genome-sequenced organisms, vs. EcYiiP. This shows that transport site A seems to be formed by lateral chains of Glu38-Asn42 in TM2 and His136-Asp150 in TM5 (Fig. 1, black dots). However, this group consists of Zn^{2+}, Cd^{2+}, Fe^{2+} and Mn^{2+} transporters of bacterial origin. Phenotypic characterization of the CDF mutant of DR_1236 in *Deinoccocus radiodurans* suggests that it transports Mn^{2+} selectively over Zn^{2+}, Fe^{2+}, Ni^{2+}, Co^{2+} and Cu^{2+} [15]. In *Synechocystis* PCC6803, the mutation of the ortholog gene Sll1263 caused a distortion in Fe homeostasis [16], while overexpression of *Thermus termophilus* CzrB in *E. coli* rendered the cells resistant to Zn^{2+} and Cd^{2+} [17]. Most of these phenotypic analyses lack the support of biochemical data by which the direction, rate and specificity of transport could be evaluated. Moreover, it has been shown that variations in Zn^{2+} levels affect intracellular Mn^{2+} concentrations [18].

In this work, we show that deletion of the gene locus SMc02724 in *S. meliloti* rendered the cells sensitive to Mn^{2+} and led to its intracellular accumulation. Resistance to Fe^{2+}, Zn^{2+}, Co^{2+} and Ni^{2+} were similar to that of the WT strain. It was possible to rescue Mn^{2+}-resistance by complementation with the gene SMc02724 under the regulation of its own promoter. Supporting a role in Mn^{2+} homeostasis, liposomes with reconstituted SmYiiP were able to specifically uptake Mn^{2+}in the presence of a H^+ gradient. Importantly, Δ*smyiiP* was unable to promote nodule formation, suggesting that Mn^{2+} homeostasis has a relevant role in establishing the nitrogen fixation process in legumes.

2. Materials and methods

2.1. Bioinformatics analyses

All sequences in the study were retrieved from the NCBI database. Alignments were performed in MUSCLE [19], and analyzed with ESPript software [20]. *E. coli* YiiP and *S. pneumonia* MntE were included in the alignment for comparison. KEGG database nomenclature was used in Fig. 1. The proteins that were not on KEGG were named with a two-letter key to denote their organismal origin as indicated in Fig. 1.

2.2. Culture media, strains and mutant constructions

S. meliloti strains were cultured in TY media (0.5% tryptone, 0.3% yeast extract, 0.09% $CaCl_2$) supplemented with streptomycin 600 μg/ml. *S. meliloti* strain Rm1021(Str^R) and *E. coli* S17-1 [21] carrying the plasmid pK19mob2ΩHMB for the mutation of SMc02714 were obtained from University of Freiburg, Germany (Table 1). The deletion mutant strain of gene SMc02724 (Δ*smyiiP*) was generated by plasmid insertion following described protocols [22]. Briefly, freshly grown *S. meliloti* Rm1021 were mixed with *E. coli* S-17 cells bearing the plasmid pK19mobΩHMB containing the internal sequence of the gene SMc02724, named G1PELR22D11 (www.rhizogate.de (GenDB)), and then incubated overnight at 30 °C on a nitrocellulose filter disk placed on top LB-agar. Conjugants were recovered from the filter and selected by plating on TY-agar supplemented with kanamycin 50–200 μg/ml. Complementation was achieved similarly by conjugation incubating the deletion mutant strain with the *E. coli* S-17 transformed with plasmid pCAP77-P-SMc02724 (Table 1). Conjugants were selected on M9 minimal media with 0.4% rhamnose as the sole carbon source [23]. The deletion and complementation of SMc02724 was checked by PCR, using primers designed to amplify the locus SMc02724 (Table 2), and purified genomic DNA as a template.

2.3. Metal sensitivity test

TY liquid cultures were inoculated at OD_{600} 0.1 from overnight cultures and supplemented with the desired $CoCl_2$, $NiCl_2$, $FeSO_4$, $ZnCl_2$ or $MnCl_2$ concentration as indicated in the figures. Cells were grown 48 h and OD_{600} was measured.

2.4. Manganese accumulation assay

Fifteen milliliters of liquid TY cultures in late exponential phase were supplemented with 0.5 mM $MnCl_2$ and incubated for 2 h. After this incubation, OD_{600} nm was determined, cells harvested, and washed with 0.9% NaCl. Pellets were digested with 0.5 ml of HNO_3 (trace

Table 2
List of primers used in this study.

Primer	Sequence (5′–> 3′)	Use
For-BamHI-Prom02724	AGCTGGATCCACCTTCGTCAACTGGCGATCC	Clone SMc02724 in pCAP77
Rev-KpnI-02724-Stop	GGTACCTCATTTCCGTGATGCTCCAC	Clone SMc02724 in pCAP77
For-NdeI-02724	TAGCTACATATGACCGGAACCGACAATAG	Clone SMc02724 in pET23b
Rev-XhoI-Tev-02724	CTCGAGGGACTGAAAATACAGGTTTTCGCCTTTCCGTGATGCTCCACTAAC	Clone SMc02724 in pET23b with TEV site

metal grade) for 1 h at 80 °C and then overnight at 20 °C. Digestions were stopped by the addition of 0.1 ml of 30% H_2O_2 and dilution to 10 ml with water. Metal contents in samples were measured by ICP–MS.

2.5. H_2O_2 sensitivity test

The TY liquid cultures were inoculated at OD_{600} of 0.1 from cells grown overnight. When an OD_{600} value of 0.6 was reached, cultures were split. One aliquot was left unamended and the other was supplemented with 0.5 mM Mn^{2+}. After 2 h the cultures were split again and 8 mM H_2O_2 was added to one aliquot. Cells (cfu/ml) were counted at 0, 30, 60, 90 and 120 min. Survival rate was estimated as the ratio of the cfu number in presence and the absence of H_2O_2.

2.6. Protein expression and purification

The gene locus SMc02724 sequence was amplified using *S. meliloti* Rm1021 genomic DNA as a template and the primers For-NdeI-02724 and Rev-XhoI-Tev-02724 (Table 2). The primers introduce NdeI and XhoI restriction sites flanking the gene and a Tobacco etch virus (TEV) protease site coding sequence at the amplicon 3′ end. The PCR product was cloned into pET23b(+) between NdeI–XhoI, which adds a six histidine tag ($(His)_6$) suitable for Ni^{2+} affinity purification. All sequences were confirmed by automated DNA sequence analysis. For heterologous expression the constructs were introduced into *E. coli* BL21(DE3)pLysS (Invitrogen). Cells were grown till mid-log phase at 37 °C in LB media supplemented with 100 μg/ml ampicillin and 33 μg/ml chloramphenicol and then induced with 0.5 mM IPTG. Cells were harvested at 4 h post-induction, washed with 25 mM Tris, pH 7.0, 100 mM KCl and stored at −70 °C. Protein purification was carried out as previously described [24]. Briefly, cells were disrupted in a bead beater (GlenMills) and membranes were isolated by centrifugation. Membranes (3 mg/ml protein) were treated with 0.75% dodecyl-ß-D-maltoside (DDM) (Calbiochem) 25 mM Tris, pH 8.0, 100 mM sucrose, 500 mM NaCl, 2 mM 2-ß-mercaptoethanol, 1 mM phenylmethylsulphonyl fluoride. The solubilized membrane protein suspension was cleared by centrifugation at 163.000 *g* for 1 h. The $(His)_6$-tagged SmYiiP protein was affinity-purified using Ni^{2+}-nitrilotriacetic acid (Ni-NTA) resin (Qiagen). After washing the resin with 5–20 mM imidazole, 50 mM Tris, pH 7.4, 0.05% DDM, 2 mM 2-ß-mercaptoethanol, the protein was eluted with 200 mM imidazole in buffer C (50 mM Tris, pH 7.4, 200 mM NaCl, 0.01% DDM, 2 mM 2-ß-mercaptoethanol) and imidazole was removed by buffer exchange (buffer C) using the Ultra-5 Centricon (Millipore) filtration device. The $(His)_6$-tag was removed from the proteins by treatment with a $(His)_6$-tagged TEV protease [24,25] at 1:1 mol:mol ratio for 2 h at 25 °C in buffer C. The TEV-His protease was removed by affinity purification with Ni-NTA resin and SmYiiP recovered in the flow through fractions. CDF his-less proteins were stored at −80 °C in buffer D2XN (25 mM Bis-Tris-Propane, pH 6.8, 100 mM NMG-MES and 2 mM 2-ß-mercaptoethanol) plus 0.01% DDM and 10% glycerol. Protein concentration was determined by Bradford [26] and BCA [27]. The mean values obtained between methods differed in less than 5%. All purification procedures were carried out at 0–4 °C, and no special precautions were taken to prevent enzyme oxidation. Purity was assessed by Coomassie Brilliant Blue staining of overloaded SDS-PAGE gels and by immunostaining Western blots with mouse anti-$(His)_6$ monoclonal primary antibody (Sigma) and goat anti-rabbit IgG secondary antibody (horseradish peroxidase conjugate; Promega).

2.7. Protein incorporation in liposomes, and transport assays

Liposomes were prepared as previously described [9] with modifications. Asolectin (Associated Concentrates, Inc.) was hydrated to a final concentration of 25 mg/ml in a buffer D (25 mM Bis-Tris-Propane, pH 6.8, 2 mM 2-ß-mercaptoethanol) by vigorous mixing on a vortex mixer. The suspension of multilamellar liposomes was sonicated in an ice-chilled bath sonicator until a clear lipid suspension was obtained, and then submitted to 3 freeze–thaw cycles from −50 °C to 20 °C. 500 μl of liposomes were destabilized adding 100 μl of 10% Triton X-100. After 5 min incubation, 400 μl of purified SmYiiP (0.1 mg/ml in buffer D2XN) plus 0.01% DDM final concentration were added and the mix incubated for 10 min. Control liposomes were made similarly, replacing protein with same volume of buffer D2XN. The mixtures were incubated 5 min at 20 °C and then detergent was removed by addition of pre-washed SM-2 Bio-beads (Bio-Rad). Bio-beads were exchanged 4 times for new ones every 15 min. The remaining Bio-beads were filtered and the volume of the sample was taken up to 8 ml with buffer DN (25 mM Bis-Tris-Propane, pH 6.8, 50 mM NMG-MES and 2 mM 2-ß-mercaptoethanol). Proteoliposomes were collected by ultracentrifugation for 100 min at 4 °C and 100.000 *g*, and finally resuspended in 200 μl of assay buffer (25 mM Bis-Tris-Propane, pH 6.8, 50 mM NMG-MES).

2.8. Fluorescent dye encapsulation into liposomes

Calcium saturated Fluo-3 was encapsulated in proteoliposomes (or control liposomes) by the freeze–thaw method. Fresh proteoliposomes were incubated for 5 min with 200 μM Fluo-3 and 200 μM $CaSO_4$ at 4 °C. The mix was sonicated for 10 s and subjected to one freeze–thaw cycle (−50 °C to room temperature) followed by an additional 10 s sonication. To remove the residual indicator from the sample, it was passed through a Sephadex G-50 column previously equilibrated with assay buffer. Loaded proteoliposomes were recovered in the void fraction.

2.9. Transition metal transport assays

The assay mixture contained 25 mM Bis-Tris-Propane, 50 mM NMG-MES, pH 6.8 (low pH assay buffer), or 7.8 (high pH assay buffer) to create a transmembrane H^+ gradient, and proteoliposomes (0.1–1 mg/ml protein). Metal uptake was initiated by the addition of 20 μM of the studied transition metal as the sulfate salt. For Fe^{2+} transport assays 0.25 mM ascorbic acid was included in the buffer. The excitation wavelength used was 485 nm and emission was measured at 535 nm. Maximal quenching (F_{max}) was obtained after disrupting the proteoliposomes with 0.1% SDS plus 2 mM metal. Data was plotted as $-\Delta F/F_{max}$ and control traces were subtracted in each case. Control liposomes showed a stable signal before and after metals were added, indicating that Ca-Fluo-3 does not undergo light quenching and that the complex remains entrapped throughout the assay. None of the reagents in the assay media produced detectable fluorescence quenching. Determinations were performed at 25 °C.

2.10. Nodulation assays

Medicago sativa seeds (alfalfa cv. Monarca obtained from Instituto Nacional de Tecnología Agropecuaria, Argentina) were surface-sterilized for 10 min with 20% (v/v) commercial bleach (equivalent to 55 g/l active Cl_2) followed by six washes with sterile distilled water. Surface-sterilized seeds were germinated inside a glass petri dish covered with cotton and filter paper. Three-day-old seedlings were aseptically planted in vermiculite pots watered sequentially with nitrogen-free Fåhraeus-modified mineral solution [28] and sterile distilled water. Plants were inoculated with exponentially grown *S. meliloti* strains (1.10^6 cfu/plant). The plants (n = 20) were cultured in a growth chamber at 25 °C with a 16/8 h photoperiod. After 28 days of growth, nodules were counted and examined and whole plants were harvested and air-dried in an oven at 70 °C for at least 48 h and the dry weights were registered. The average number of nodules per plant and the average dry weight for each treatment were obtained.

3. Results

3.1. SmYiiP is required for Mn^{2+} homeostasis in S. meliloti

Bacterial CDF transporters are involved in transition metal homeostasis driving their cytosolic efflux to external compartments [6]. Genome analysis of *S. meliloti* shows two paralogous genes coding for CDF transporters, SMc02724 and SMc04147. Recent bioinformatics studies have shown that orthologs of SMc04147 are involved in Co^{2+} and Ni^{2+} homeostasis in *S. etli* [14]. The same analysis predicts broad transport specificity for SMc02724. However, in *D. radiodurans*, the ortholog gene DR_1236 is responsible only for Mn^{2+} homeostasis [15]. To evaluate the role of SMc02724 in *S. meliloti*, the deletion mutant Δ*smyiiP* was generated and its sensitivity to Co^{2+}, Ni^{2+}, Zn^{2+}, Fe^{2+} and Mn^{2+} were analyzed. The deletion mutant showed increased sensitivity towards Mn^{2+} (Fig. 2A) and similar sensitivity to Co^{2+}, Zn^{2+}, Ni^{2+} or Fe^{2+} compared to the parental strain (WT) (Fig. 2B–E). Higher concentrations of Mn^{2+} and Fe^{2+} were required to stop cell growth compared to Zn^{2+}, Co^{2+} and Ni^{2+}, probably reflecting the lower stability constants for the Mn/Fe-protein abducts. Importantly, the complemented strain Δ*smyiiP rhaS::P-smyiiP* attained similar levels to those of WT, discarding polar effects.

Given the putative function for SMc02724 as a transition metal exporter and the Mn^{2+}-sensitive phenotype observed, we hypothesized that Mn^{2+} accumulation in Δ*smyiiP* strain must affect normal cell growth. Hence, it is predicted that Mn^{2+} accumulation may occur in cells grown at sub-lethal Mn^{2+} concentrations. To test this, strains Δ*smyiiP* and WT were grown in the presence of 0.5 mM Mn^{2+} in TY medium. Compared to WT, strain Δ*smyiiP* almost doubled the amount of intracellular Mn^{2+} (Fig. 3A).

In *S. pneumonia* deletion of MntE led to Mn^{2+} accumulation and decreased ROS sensitivity [13]. To test a similar effect we compared the survival rates of WT and Δ*smyiip* strains in presence of H_2O_2 and observed no differences (Fig. 3B, empty symbols). Pre-incubation of cells with a sub-lethal Mn^{2+} concentration of 0.5 mM for 2 h before the H_2O_2 addition resulted in similar survival rates between the Δ*smyiip* and the WT strain (Fig. 3B, filled symbols).

3.2. Specific Mn^{2+} transport by SmYiiP requires a transmembrane H^+ gradient

Several membrane proteins of *S. meliloti* are involved in transition metal efflux. ActP (CopA), ZntA and Nia, members of the PIB-ATPases family, participate in Cu^{+}, Zn^{2+} and Fe^{2+} homeostasis, respectively [29–31]. Our in vivo assay data indicate that the cognate metal for SmYiiP would be Mn^{2+}. To test this in vitro, we measured Mn^{2+}, Fe^{2+}, Co^{2+}, Ni^{2+} and Zn^{2+} uptake in liposomes containing SmYiiP. SmYiiP was heterologously expressed in *E. coli* and purified by Ni-NTA affinity chromatography. It is known that $(His)_6$-tag binds divalent cations like Co^{2+} and Ni^{2+}. Thus, to avoid any interference in the uptake assay, a TEV site was inserted between the protein sequence and the $(His)_6$-tag to remove it via TEV-$(His)_6$-tagged protease treatment. After the treatment, the $(His)_6$-less SmYiiP was re-purified by reversed Ni-NTA purification (Fig. 4A). Protein analysis by Coomassie blue staining and Western blot showed that the protein recovered in the flow-through corresponds to the $(His)_6$-less version of SmYiiP, as an anti-

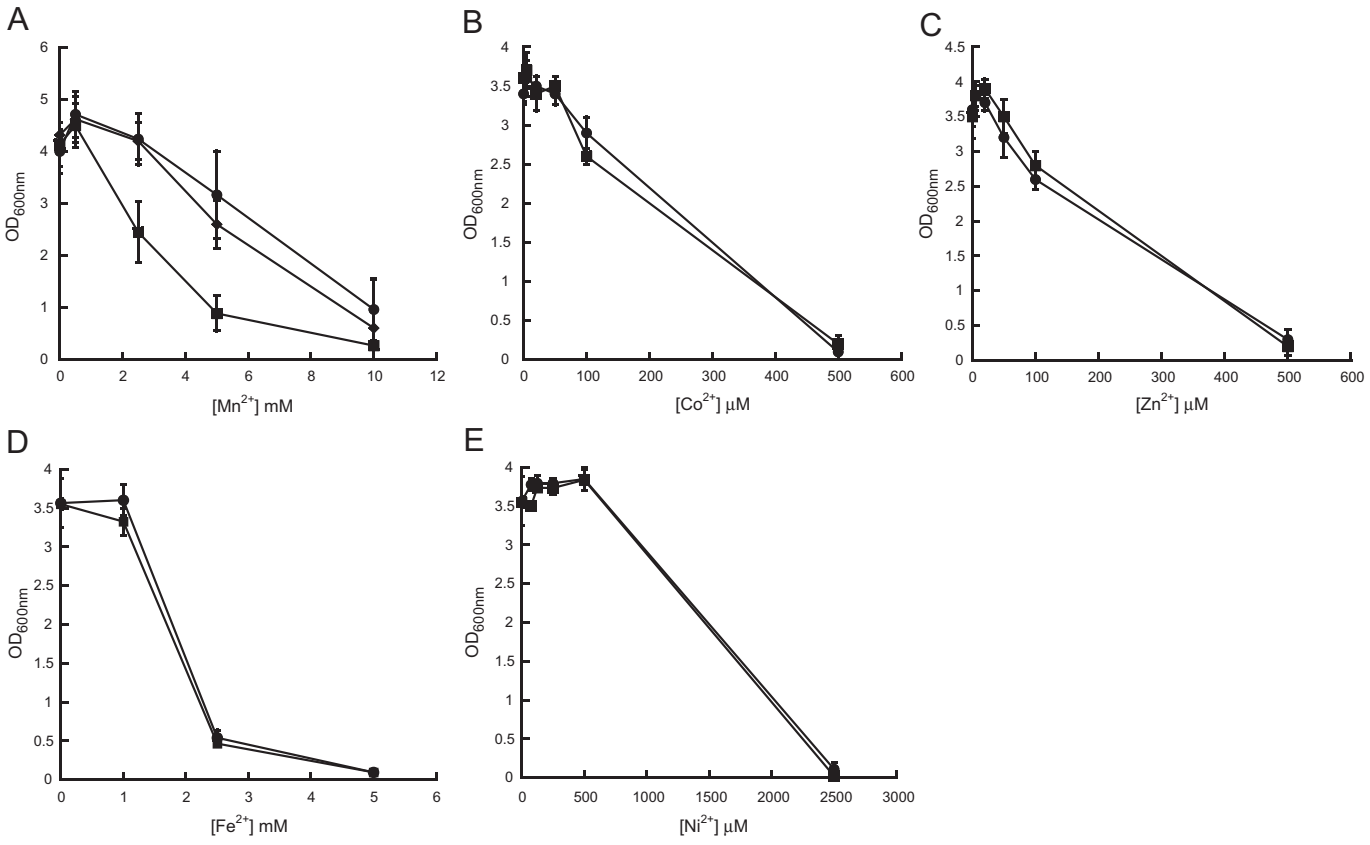

Fig. 2. Roles of SmYiiP in Mn^{2+}, Co^{2+}, Zn^{2+}, $Fe^{2+}$and Ni^{2+} tolerance. Manganese (A), cobalt (B) zinc (C), iron (D) and nickel (E) sensitivity of *S. meliloti* Rm1021 (circle), the deletion mutant of SMc02724 (Δ*smyiiP*) (square), and the deletion mutant of SMc02724 complemented in cis- with SMc02724 under the regulation of its own promoter (Δ*smyiiP rhaS::P-smyiiP*) (diamond). Cells were cultured for 48 h in liquid TY medium in the presence of different metal concentrations as indicated and the OD_{600} was measured. Data are the mean ± SE of three independent experiments.

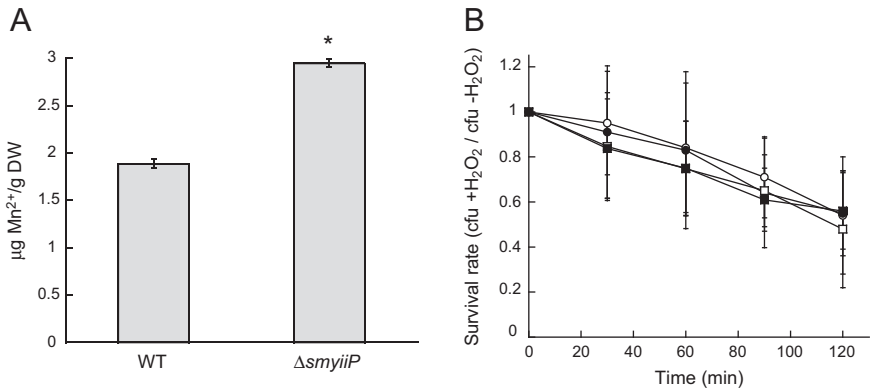

Fig. 3. SmYiip is involved in Mn^{2+} homeostasis. (A) Manganese content was measured in *S. meliloti* Rm1021 (WT) and Δ*smyiiP*. Cells were exposed to 0.5 mM $MnCl_2$ for 2 h. Data are the mean ± SE of three independent experiments. * $p < 0.05$ vs. WT. (B) Cell survival of *S. meliloti* Rm1021 (circles) and Δ*smyiiP* (squares) was determined after the addition of 8 mM H_2O_2 to cells pre-incubated (filled symbols) or not (empty symbols) with 0.5 mM Mn^{2+} in TY medium for indicated lengths of time. Cell survival is shown as the ratio of cfu determined in H_2O_2 treated/untreated cultures. Data are the mean ± SE of three independent experiments.

$(His)_6$ antibody was unable to detect it (Fig. 4A, lanes 2 and 4). SmYiiP was then incorporated into asolectin liposomes to evaluate its transport activity and functionality. To detect divalent metal uptake into the liposomes, these were loaded with 200 µM of Fluo-3 and 200 µM of Ca^{2+}. Untrapped dye was removed by molecular filtration using Sephadex G-50, and the quenching of fluorescence of the Ca-Fluo-3 complex was followed using $\lambda_{exc} = 485$ nm and $\lambda_{em} = 535$ nm, before and after the addition of each candidate metal to the liposomes. A similar approach was used to detect Nramp-mediated Mn^{2+}, Co^{2+} and Fe^{2+} import in human cells [32], based on the quenching of the emission signal of a fluorescent dye saturated with Ca^{2+} when this is displaced by a transition metal with a higher stability constant (i.e., K_d Ca-Fluo-3 = 400 nM vs. K_d Mn-Fluo-3 = 7nM). Fig. 4 shows the steady state fluorescence quenching mediated by the addition of 20 µM metal plotted as the $-\Delta F/F_{max}$. Fluorescence traces in liposomes with no protein were subtracted in each case. A higher rate of quenching of the Ca-Fluo-3 emission signal was observed upon addition of all candidate metals under the no H^+ gradient condition (pH 6.8 inside, pH 6.8 outside)(Fig. 4B–F, filled symbols). It is accepted that CDF mediated metal transport in vivo is coupled to the down-hill transport of H^+. Therefore, a ΔpH metal dependent transport would represent the cellular scenario revealing probably a preference for a metal candidate as the transported substrate. We first tested the ΔpH stability across liposomes (pH 6.8 inside, pH 7.8 outside). In our assay conditions we observed no changes in the fluorescent pyranine emission signal meaning that the ΔpH remains steady (Supplementary Fig. 1) until the metal uptake reaction was started. Surprisingly, the Mn^{2+} uptake rate was increased in the high pH assay buffer (pH 6.8 inside, pH 7.8 outside) (Fig. 4B, empty symbols) and the rates of Co^{2+}, Zn^{2+}, Fe^{2+} and Ni^{2+} remained unchanged (Fig. 4C–F, empty symbols). Thus, the Mn^{2+} transport could be defined as ΔpH-dependent and the results support the in vivo findings that point to SmYiiP as a Mn^{2+} exporter. However, as discussed later, other mechanisms could also limit the role of SmYiiP only to Mn^{2+} homeostasis.

3.3. SmYiiP is required for full nodulation capacity

It has previously been demonstrated that intracellular Mn^{2+} is key in *S. meliloti* to avoid nodule senescence [33], and that its ion levels could affect initial stages of infection [34]. In order to promote nodulation in alfalfa roots, *S. meliloti* has to overcome redox stress imposed by the plant to colonize the roots [35]. To test the role of SmYiiP in nodulation, 2–3 day old alfalfa seedlings were inoculated with 1.10^6 cfu/plant of *S. meliloti* WT, Δ*smyiiP* or Δ*smyiiP rhaS::P-smyiiP*. Fig. 5A shows the number of nodules at 28 dpi. There was a decrease in the number of nodules in plants infected with the strain Δ*smyiiP*, which correlated with a lighter weight and a smaller plant size shown by these plants compared to WT and the complemented strain Δ*smyiiP rhaS::P-smyiiP* (Fig. 5B and C). Whether the phenotype observed is the consequence of non-functional senescent nodules (fix-) or of defective bacterial infection (nod-) requires further investigation.

4. Discussion

The functional roles of bacterial CDF family members have been assigned to transition metal homeostasis [6,7]. Previous findings, such as decreased resistance to a specific transition metal and its intracellular accumulation in strains lacking functional CDFs, led to this proposition. Mechanistically, it is hypothesized that transmembrane transport is driven by conformational changes induced by the cognate metal when bound to the transport site and the presence of H^+ gradient [10,11]. Although the capacity to transport specific metals has been proven to be linked to structural factors, such as the geometry of coordination at the entry, transport and exit sites of the transporter, other determinants for specificity might be present in the transport mechanism prior to the metal binding to the transporter. The observed transport in the absence of H^+ gradient suggests that the unspecific metal binding is thermodynamically and kinetically possible, but this is not translated to functionality in vivo. As mentioned, not only the binding of these metals to the regulatory sites (Site B and C), but also the possible physical interactions of the transporter with specific metal pools via small chelating compounds or metallochaperones seem to contribute to achieving the specificity for Mn^{2+} observed in vivo.

An important experimental evidence highlights the fact that proton countertransport is determinant to attain specificity. Only the transport rate of Mn^{2+} was increased in the presence of a H^+ gradient, while the transport rate of the other metals remains unchanged (Fig. 4). A recent structural study of the *E. coli* CDF member indicates that different H^+ concentrations across membrane promotes conformational changes in TMD assuring the substrate vectorial transport [36]. In a similar fashion asymmetric H^+ concentrations might induce conformational changes to attain Mn^{2+} binding to the transport site.

Transition metals, and consequently metal transporters, play an essential role in biological nitrogen fixation (BNF), and even more in the rhizobium–legume symbiosis. They are cofactors of the enzymatic machinery directly responsible for BNF (nitrogenase, ferredoxin, etc.), and of many of the enzymes directed to reactive oxygen species (ROS) control. However, very little is known about the role of bacterial metal transporters in BNF. Early stages of infection are highly dependent on ROS generation in the plant [33,35] and transition metals are likely involved in ROS generation in plants, as well as in ROS clearance in bacteria. Although there is little evidence, transition metals could be part of

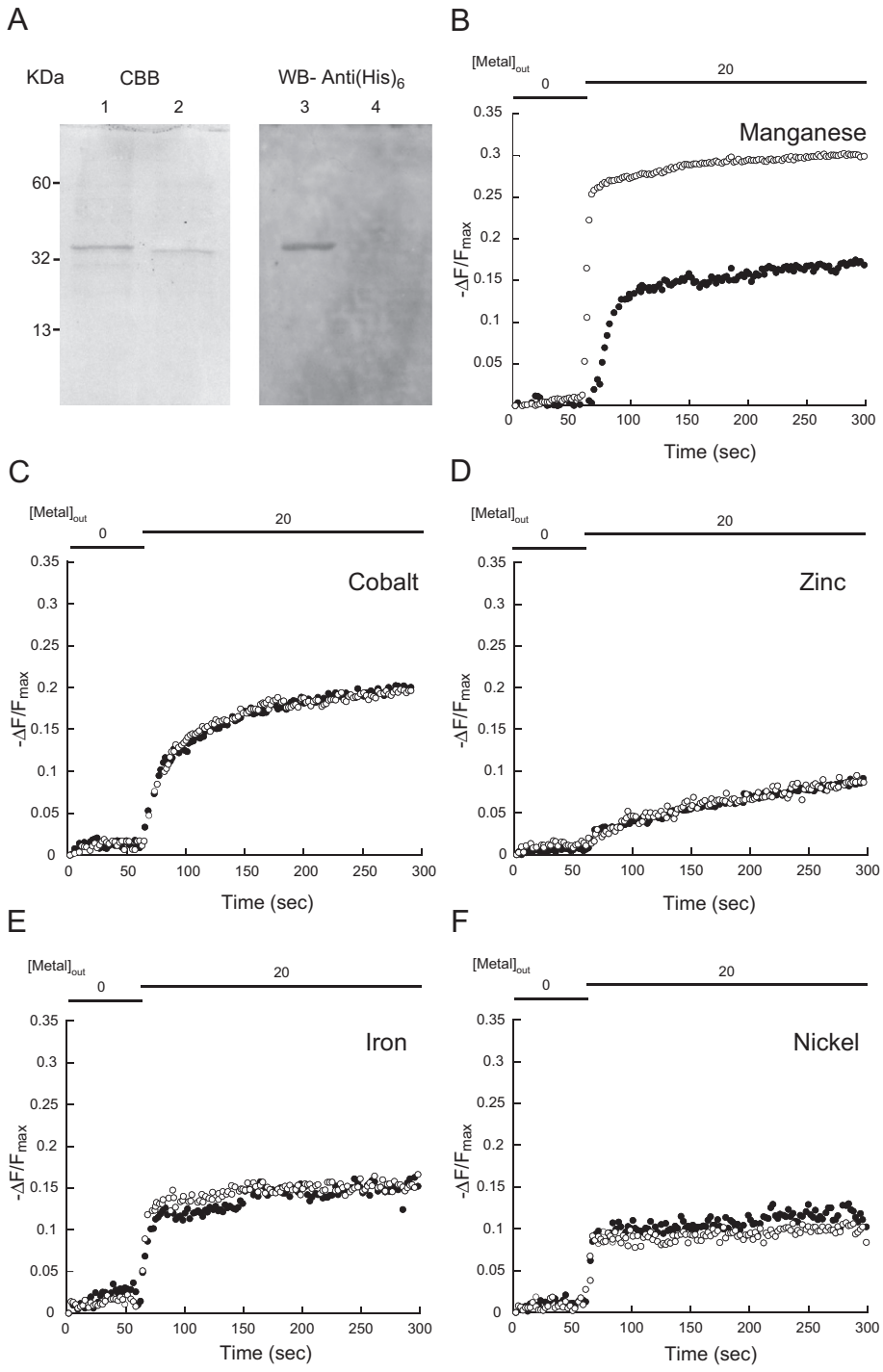

Fig. 4. In vitro SmYiiP transition metal transport in the presence and absence of H^+ gradient. (A) $(His)_6$-tagged SmYiiP was purified by Ni-NTA (lanes 1 and 3). After TEV protease treatment $(His)_6$-less SmYiiP was obtained by reversed Ni-NTA affinity chromatography in the flow-through fraction (lanes 2 and 4) and incorporated in liposomes for metal transport measurement. CBB, Coomassie brilliant blue staining; WB-Anti-$(His)_6$, Western blot with monoclonal anti-$(His)_6$ tag. Metal transport was measured in the presence (pH 6.8 inside, pH 7.8 outside; empty symbol) or absence (pH 6.8 inside, pH 6.8 outside; filled symbol) of a H^+ diffusion gradient by the addition (as sulfate) of (B) Mn^{2+},(C) Co^{2+}, (D) Zn^{2+}, (E) Fe^{2+} and (F) Ni^{2+} to proteoliposomes with $(Hiss)_6$-less SmYiiP incorporated. Metals were added at 60 s to a final outside concentration of 20 μM ($[Metal]_{out}$). Traces represent the total $-\Delta F/F_{max}$ after control liposome signals were subtracted.

environmental factors altering the establishment of the rhizobium–plant symbiosis [34].

Our results indicate that SmYiiP activity maintains cytosolic Mn^{2+} levels compatible with cell growth. In *S. pneumonia*, accumulation of intracellular Mn^{2+} due to the lack of function of the CDF transporter MntE played a protective role against ROS [13]. In our hands, the resistance to ROS of the Δ*smyiiP* strain was similar to that of the WT even in presence of Mn^{2+}.

It is also likely that the lack of function of SmYiiP affects important initial steps during the *S. meliloti*-plant recognition phase, or later, the physiological metabolism in the bacteroid inside nodules. A decrease in the number of nodules was found in plants inoculated with Δ*smyiiP* and, although the morphological appearance of nodules was normal compared to those induced by WT, we cannot discard a reduction in their functionality. It has been noted that Mn^{2+}-limited rhizobial cells were most effective in hair root adhesion [34]. Thus, we speculate that

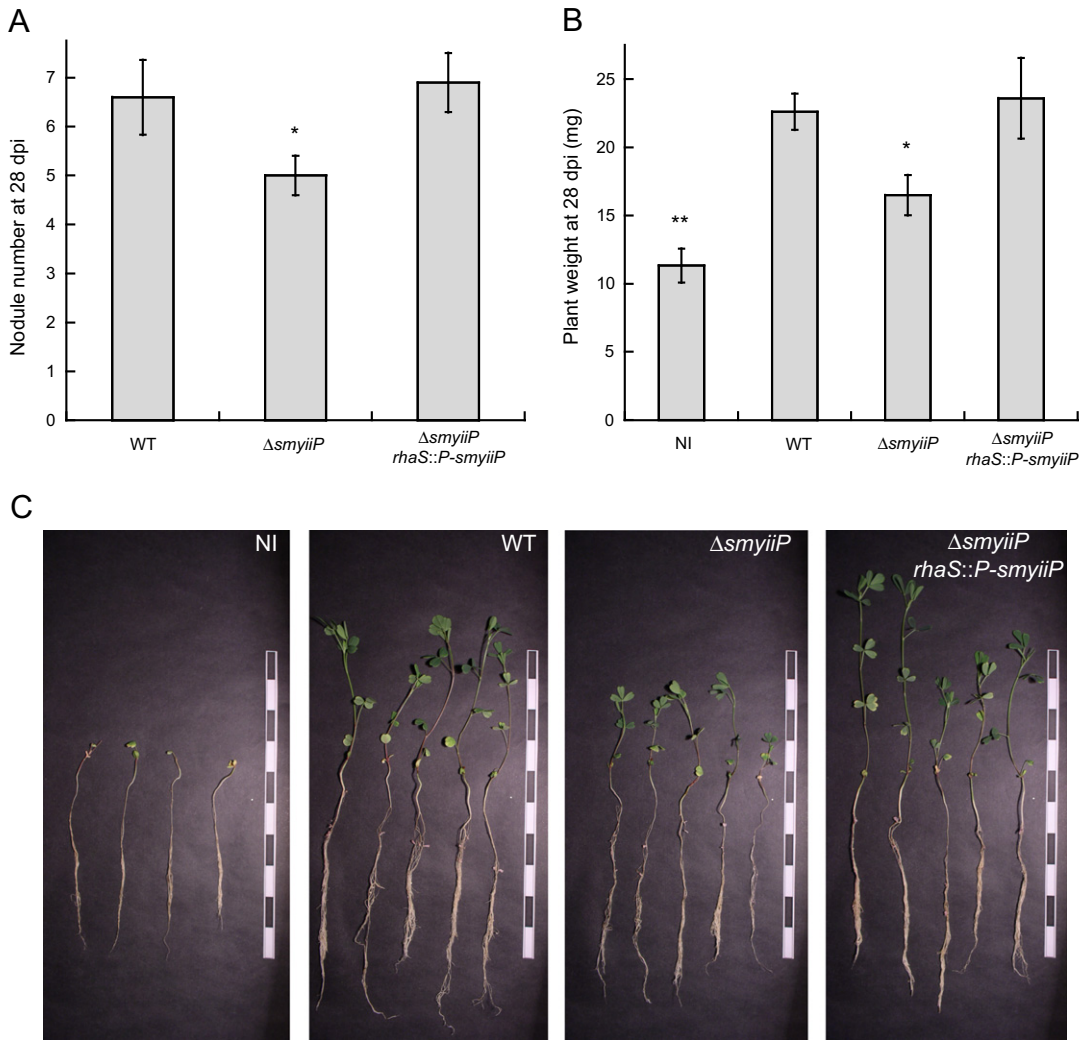

Fig. 5. SmYiiP role during alfalfa infection and nodulation. 3-day-old alfalfa seedlings grown in vermiculite were inoculated with the same number (1.10^6 cfu) of *S. meliloti* Rm1021 (WT), deletion mutant of SMc02724 (Δ*smyiiP*), or the deletion mutant of SMc02724 complemented in cis- with SMc02724 under the regulation of its own promoter (Δ*smyiiP rhaS::P-smyiiP*). (A) Nodules per plant at 28-day post infection (dpi). (B) Dried plant weight at 28 dpi. NI, non-inoculated plants. Data are the mean ± SE of two independent experiments (n = 20). * $p < 0.05$ vs. WT and ** $p < 0.005$ vs. WT. (C) Representative alfalfa plant growth in vermiculite at 28 dpi with different strains. Black and white scale bars = 2 cm.

a subtle increase in cytosolic Mn^{2+} in Δ*smyiiP* interferes with signaling for infection at the early stages. Although in our experimental condition no exogenous Mn^{2+} was added other than that contained in the Fåhraeus solution, it has been shown that a significant amount of Mn found in vermiculite might become available as micronutrient for soil growing bacteria [37]. Indicating the importance of Mn^{2+} at the last stages of infection, ABC-family importers involved in Mn^{2+} uptake were reported to occur in bacteroid cells [33].

4.1. Conclusions

The present study demonstrated the participation of the *S. meliloti* SmYiiP transporter in Mn^{2+} homeostasis as an exporter in the cytosolic membrane. Infection of plants inoculated with the *S. meliloti* strain lacking SmYiiP was affected, resulting in a decreased number of nodules. These results support the relevance of Mn^{2+} homeostasis as a key factor for BNF in legumes.

Supplementary data to this article can be found online at http://dx.doi.org/10.1016/j.bbamem.2014.09.005.

Acknowledgments

This work was supported by the Consejo Nacional de Investigaciones Científicas y Tecnológicas (CONICET-G111220090100063 to G.E.) (Subsidio extraordinario to D.R.). G. E. is an established CONICET investigator. D. R. is a CONICET career investigator. We are grateful to Dr. Daniel Gage (University of Connecticut, USA) and Dr. Ancke Becker (Center for Biotechnology, University of Bielefeld, Germany) for strains and plasmids to generate *S. meliloti* strains. We thank Dr. Daniel Basigalup (INTA, Argentina) for providing us with alfalfa seeds and Myriam Siravegna for technical support.

References

[1] D. Osman, J.S. Cavet, Copper homeostasis in bacteria, Adv. Appl. Microbiol. 65 (2008) 217–247.
[2] L. Macomber, J.A. Imlay, The iron-sulfur clusters of dehydratases are primary intracellular targets of copper toxicity, Proc. Natl. Acad. Sci. U. S. A. 106 (2009) 8344–8349.
[3] C. Ranquet, S. Ollagnier-de-Choudens, L. Loiseau, F. Barras, M. Fontecave, Cobalt stress in *Escherichia coli*. The effect on the iron–sulfur proteins, J. Biol. Chem. 282 (2007) 30442–30451.
[4] M. González-Guerrero, D. Raimunda, X. Cheng, J.M. Argüello, Distinct functional roles of homologous Cu^+ efflux ATPases in *Pseudomonas aeruginosa*, Mol. Microbiol. 78 (2010) 1246–1258.
[5] D. Raimunda, M. González-Guerrero, B.W. Leeber III, J.M. Argüello, The transport mechanism of bacterial Cu^+-ATPases: distinct efflux rates adapted to different function, Biometals 24 (2011) 467–475.
[6] D.H. Nies, Efflux-mediated heavy metal resistance in prokaryotes, FEMS Microbiol. Rev. 27 (2003) 313–339.
[7] G. Grass, M. Otto, B. Fricke, C.J. Haney, C. Rensing, D.H. Nies, D. Munkelt, FieF (YiiP) from *Escherichia coli* mediates decreased cellular accumulation of iron and relieves iron stress, Arch. Microbiol. 183 (2005) 9–18.

[8] A.A. Guffanti, Y. Wei, S.V. Rood, T.A. Krulwich, An antiport mechanism for a member of the cation diffusion facilitator family: divalent cations efflux in exchange for K^+ and H^+, Mol. Microbiol. 45 (2002) 145–153.
[9] Y. Chao, D. Fu, Kinetic study of the antiport mechanism of an *Escherichia coli* zinc transporter, ZitB, J. Biol. Chem. 279 (2004) 12043–12050.
[10] M. Lu, J. Chai, D. Fu, Structural basis for autoregulation of the zinc transporter YiiP, Nat. Struct. Mol. Biol. 16 (2009) 1063–1067.
[11] N. Coudray, S. Valvo, M. Hu, R. Lasala, C. Kim, M. Vink, M. Zhou, D. Provasi, M. Filizola, J. Tao, J. Fang, P.A. Penczek, I. Ubarretxena-Belandia, D.L. Stokes, Inward-facing conformation of the zinc transporter YiiP revealed by cryoelectron microscopy, Proc. Natl. Acad. Sci. U. S. A. 110 (2013) 2140–2145.
[12] E. Hoch, W. Lin, J. Chai, M. Hershfinkel, D. Fu, I. Sekler, Histidine pairing at the metal transport site of mammalian ZnT transporters controls Zn^{2+} over Cd^{2+} selectivity, Proc. Natl. Acad. Sci. U. S. A. 109 (2012) 7202–7207.
[13] J.W. Rosch, G. Gao, G. Ridout, Y.D. Wang, E.I. Tuomanen, Role of the manganese efflux system *mntE* for signalling and pathogenesis in *Streptococcus pneumoniae*, Mol. Microbiol. 72 (2009) 12–25.
[14] C. Cubillas, P. Vinuesa, M.L. Tabche, A. Garcia-de los Santos, Phylogenomic analysis of cation diffusion facilitator proteins uncovers Ni^{2+}/Co^{2+} transporters, Metallomics 5 (2013) 1634–1643.
[15] H. Sun, G. Xu, H. Zhan, H. Chen, Z. Sun, B. Tian, Y. Hua, Identification and evaluation of the role of the manganese efflux protein in *Deinococcus radiodurans*, BMC Microbiol. 10 (2010) 319.
[16] H.B. Jiang, W.J. Lou, H.Y. Du, N.M. Price, B.S. Qiu, Sll1263, a unique cation diffusion facilitator protein that promotes iron uptake in the cyanobacterium *Synechocystis* sp. Strain PCC 6803, Plant Cell Physiol. 53 (2012) 1404–1417.
[17] S. Spada, J.T. Pembroke, J.G. Wall, Isolation of a novel *Thermus thermophilus* metal efflux protein that improves *Escherichia coli* growth under stress conditions, Extremophiles 6 (2002) 301–308.
[18] F.E. Jacobsen, K.M. Kazmierczak, J.P. Lisher, M.E. Winkler, D.P. Giedroc, Interplay between manganese and zinc homeostasis in the human pathogen *Streptococcus pneumoniae*, Metallomics 3 (2011) 38–41.
[19] R.C. Edgar, MUSCLE: multiple sequence alignment with high accuracy and high throughput, Nucleic Acids Res. 32 (2004) 1792–1797.
[20] P. Gouet, E. Courcelle, D.I. Stuart, F. Metoz, ESPript: analysis of multiple sequence alignments in PostScript, Bioinformatics 15 (1999) 305–308.
[21] R. Simon, U. Priefer, A. Puhler, A broad host range mobilization system for in vivo genetic engineering: transposon mutagenesis in gram negative bacteria, Nat. Biotechnol. 1 (1983) 784–791.
[22] L. Luo, S.Y. Yao, A. Becker, S. Ruberg, G.Q. Yu, J.B. Zhu, H.P. Cheng, Two new *Sinorhizobium meliloti* LysR-type transcriptional regulators required for nodulation, J. Bacteriol. 187 (2005) 4562–4572.
[23] C. Arango Pinedo, D.J. Gage, Plasmids that insert into the rhamnose utilization locus, *rha*: a versatile tool for genetic studies in *Sinorhizobium meliloti*, J. Mol. Microbiol. Biotechnol. 17 (2009) 201–210.
[24] D. Raimunda, P. Subramanian, T. Stemmler, J.M. Argüello, A tetrahedral coordination of Zinc during transmembrane transport by P-type Zn^{2+}-ATPases, Biochim. Biophys. Acta 1818 (2012) 1374–1377.
[25] S. van den Berg, P.A. Lofdahl, T. Hard, H. Berglund, Improved solubility of TEV protease by directed evolution, J. Biotechnol. 121 (2006) 291–298.
[26] M.M. Bradford, A rapid and sensitive method for the quantitation of microgram quantities of protein utilizing the principle of protein–dye binding, Anal. Biochem. 72 (1976) 248–254.
[27] P.K. Smith, R.I. Krohn, G.T. Hermanson, A.K. Mallia, F.H. Gartner, M.D. Provenzano, E.K. Fujimoto, N.M. Goeke, B.J. Olson, D.C. Klenk, Measurement of protein using bicinchoninic acid, Anal. Biochem. 150 (1985) 76–85.
[28] A.R. Lodeiro, P. Gonzalez, A. Hernandez, L.J. Balague, G. Favelukes, Comparison of drought tolerance in nitrogen-fixing and inorganic nitrogen-grown common beans, Plant Sci. 154 (2000) 31–41.
[29] S. Rossbach, D.J. Mai, E.L. Carter, L. Sauviac, D. Capela, C. Bruand, F.J. de Bruijn, Response of *Sinorhizobium meliloti* to elevated concentrations of cadmium and zinc, Appl. Environ. Microbiol. 74 (2008) 4218–4221.
[30] S.J. Patel, T. Padilla-Benavides, J.M. Collins, J. Arguello, Functional diversity of five homologous Cu + -ATPases present in *Sinorhizobium meliloti*, Microbiology 160 (2014) 1237–1251.
[31] E.L. Zielazinski, M. González-Guerrero, P. Subramanian, T.L. Stemmler, J.M. Argüello, A.C. Rosenzweig, *Sinorhizobium meliloti* Nia is a P(1B-5)-ATPase expressed in the nodule during plant symbiosis and is involved in Ni and Fe transport, Metallomics 5 (2013) 1614–1623.
[32] J.R. Forbes, P. Gros, Iron, manganese, and cobalt transport by Nramp1 (Slc11a1) and Nramp2 (Slc11a2) expressed at the plasma membrane, Blood 102 (2003) 1884–1892.
[33] B.W. Davies, G.C. Walker, Disruption of *sitA* compromises *Sinorhizobium meliloti* for manganese uptake required for protection against oxidative stress, J. Bacteriol. 189 (2007) 2101–2109.
[34] J.W. Kijne, G. Smit, C.L. Diaz, B.J. Lugtenberg, Lectin-enhanced accumulation of manganese-limited *Rhizobium leguminosarum* cells on pea root hair tips, J. Bacteriol. 170 (1988) 2994–3000.
[35] S.K. Ramu, H.M. Peng, D.R. Cook, Nod factor induction of reactive oxygen species production is correlated with expression of the early nodulin gene *rip1* in *Medicago truncatula*, Mol. Plant Microbe Interact. 15 (2002) 522–528.
[36] S. Gupta, J. Chai, J. Cheng, R. D'Mello, M.R. Chance, D. Fu, Visualizing the kinetic power stroke that drives proton-coupled zinc(II) transport, Nature 512 (2014) 101–104.
[37] B. Müller, Impact of the bacterium *Pseudomonas fluorescens* and its genetic derivatives on vermiculite: effects on trace metals contents and clay mineralogical properties, Geoderma 153 (2009) 94–103.